Lawrence Berkeley Laboratory
UNIVERSITY OF CALIFORNIA

Materials & Molecular Research Division

Submitted to Wear

THE PLATELET MECHANISM OF EROSION OF DUCTILE METALS

A.V. Levy

May 1984

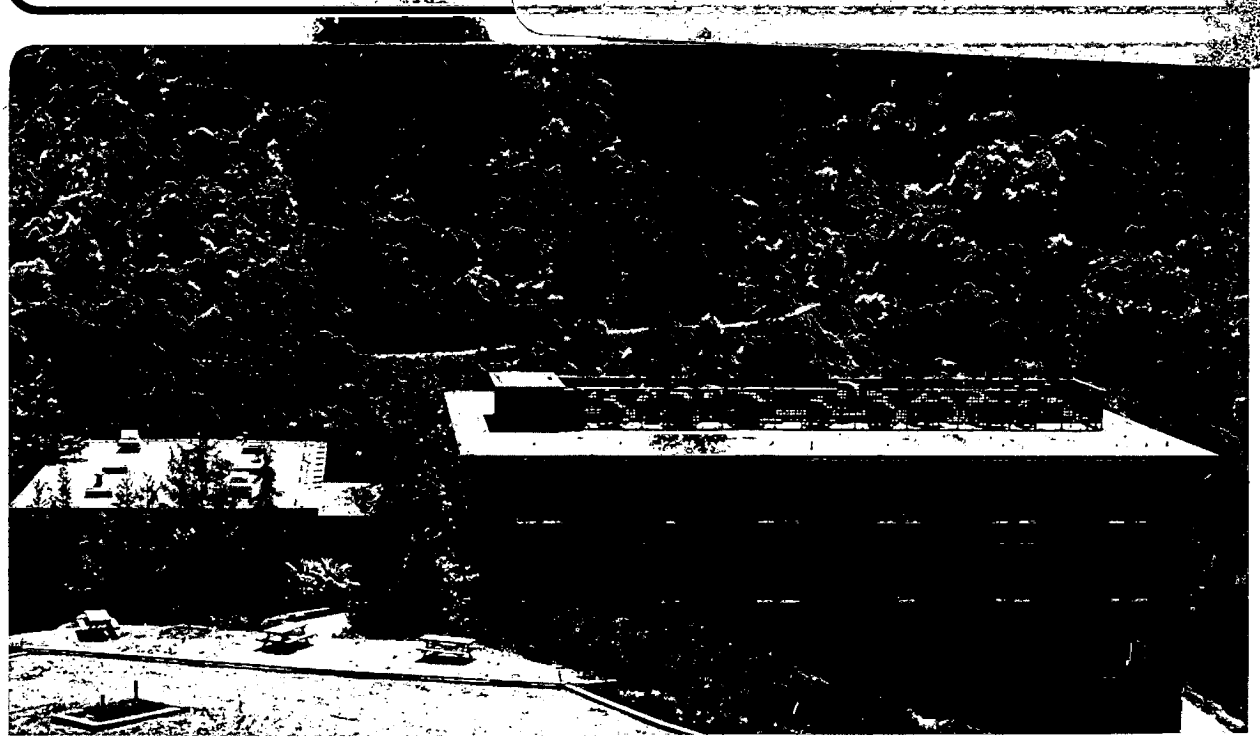

Prepared for the U.S. Department of Energy under Contract DE-AC03-76SF00098

DISCLAIMER

LBL-15240 Rev.

THE PLATELET MECHANISM OF EROSION OF DUCTILE METALS

Alan V. Levy

Materials and Molecular Research Division
Lawrence Berkeley Laboratory
University of California
Berkeley, California 94720

This work is supported by the Technical Coordination Staff of the Office of Fossil Energy of the U.S. Department of Energy under Contract Number DE-AC03-76SF00098 through the Fossil Energy Materials Program, Oak Ridge National Laboratory, Oak Ridge, Tennessee.

ABSTRACT

A platelet mechanism of erosion for ductile metals is defined and evidence of its validity is presented. The effects of the plastic deformation characteristics of metals on their erosion by particles carried in gas streams is reviewed and related to the proposed erosion mechanism. The data presented indicates that erosion of ductile metals was related to properties of alloys such as ductility, strain hardening coefficient and some thermal properties that have not previously been considered in selecting alloys for erosion service. Hardness and strength do not relate to erosion resistance in the manner usually prescribed to them.

INTRODUCTION

Structural metals have had surface material removed in service as the result of erosion by small, solid, impacting particles in many types of service. Through the years particular engineering problems have arisen that temporarily intensified erosion research. Among them have been catalytic cracker erosion from catalyst pellets, turbine engine compressor blade erosion from sand ingestion in helicopter engines and char particle erosion in coal gasifiers. Until 1958 much of the work carried out to obtain erosion information was empirical. In 1958 Finnie developed an analytical model to attempt to predict erosion rates that was based on the assumption that the mechanism of erosion was micro-machining.[1] Based on the primary assumption that the eroding particles cut swaths of metal from the alloy as their tips translated along the eroding surface, the basis for the analytical model was an equation of motion of the tips of the particles. By

analytically describing the path of the particle and assuming that the volume of metal removed was the product of the area swept out by the particle tip and the width of the cutting face,metal removal by the erosion process was accounted for.[2]

This basic assumption of the model of micro-machining of the target metal by the tips of the eroding particles was faulted by not being able to predict several important aspects of the measured erosion loss. These included the accurate effect of particle velocity (its exponent in the model), the occurrence of considerable weight loss near an impingement angle of 90° (model predicts no erosion at 90°) and the impingement angle where maximum erosion occurs (experimental curves had to be moved to make the measured angle and the predicted angle coincide). In recent work a mounting body of evidence has demonstrated that micro-machining is not the mechanism by which ductile structural metals erode. This evidence will be presented in this paper.

The other major consideration in the erosion of ductile metals that has been widely accepted for many years is the effect of hardness/strength. Based upon the erosion behavior of the elemental metals, it was thought that higher hardness results in greater erosion resistance.[3] This basic premise has also been disproved for metallic alloys in recent work.[16,17]

This paper is intended to bring together a body of evidence that supports a mechanism of erosion that is based upon micro-extrusion and forging rather than machining. It was developed as the result of observations of erosion surfaces using the scanning electron

microscope (SEM) at high magnifications with great depth of field. Some of the figures utilized in this paper are from work published earlier by the author. They have been incorporated because they are particularly important to the continuity of the review. The papers in which they initially appeared are referenced. The mechanism is in agreement with those aspects of erosion behavior that the micro-machining mechanism of erosion could not account for as well as those that it did explain. While the new mechanism of erosion has not yet been reduced to a predictive model, it has been developed far enough to indicate some of the properties of ductile alloys that do and do not enhance erosion resistance.

THE PLATELET MECHANISM OF EROSION

A review of the evolution of the platelet mechanism of erosion of ductile metals by small solid particles will be helpful in making the transition from the micro-machining mechanism. In work conducted by the author to determine how specific steel microstructures affected erosion, an erosion weight loss technique was used that caused the basic doubt about the validity of the micro-cutting mechanism.[4] In order to learn more about the initiation of erosion, an incremental weight loss measurement rather than the cumulative one generally reported in the literature was used. The erosion was conducted incrementally, 60gm of particles at a time, and the weight loss caused by each 60gm increment was determined and plotted as shown in Figure

1. It can be seen that the initial erosion rate caused by the first 60gm of SiC particles was much lower than that of subsequent 60gm batches of erodent.

Also, extrapolating the curves down to 0 erosion indicates that a number of grams of particles have impacted the surface before weighable erosion losses commence. If micro-machining was the mechanism of erosion, the erosion rate of the initial, uneroded surface should be higher than subsequent incremental rates where work hardening of the surface due to the machining action would have reduced the machineability of the surface. Erosion also should have started with the first impinging particles. Neither of these accurrences was measured, see Figure 1.

It can also be seen in Figure 1 that doubts concerning the effect of hardness and strength effects on erosion were also raised. The lowest hardness, lowest strength condition of the 1075 eutectoid steel, the spheroidized condition, had the lowest erosion rate.

The effect of work hardening of the spheroidized steel was also investigated.[4] It was initially expected that as the material was worked hardened, its erosion resistance would increase with the resulting hardness increase. Table 1 shows the erosion rate for the initial 60gm of erodent for spheroidized 1075 steel specimens that were cold rolled to various percentage reductions prior to eroding them. The hardness doubled between the annealed steel and the 80% cold reduced steel, but the erosion rate, rather than decreasing with increasing hardness, increased significantly. It did not achieve the steady state incremental erosion rate shown in figure 1, but

approached it.

These two pieces of evidence coupled with scanning electron microscope (SEM) photomicrographs showing extensive piling up of material around craters produced by single particle impacts, Figure 2, established doubts regarding the micro-machining mechanism of erosion. These doubts were reinforced by Figure 3. It shows, at low magnification, the region at the edge of the primary erosion zone of 1100-0 aluminum that was eroded to the steady state condition by spherical steel shot at a relatively steep impingement angle, $\alpha = 60^{o}$ and a velocity of 30 m/s. Many platelets can be seen that were made by an extrusion-forging action much the same as occurs when a soft, malleable metal like gold is beat with a ball peen hammer. Some of the platelets are bent, indicating that another impact on them could break off the bent part or even the whole platelet.

Microscopic Sequences

A technique was developed to metallographically observe the development of an eroded surface a few impacts at a time.[5] The same micro area was observed in the SEM after sequential, very short erosion exposures. Small, 300-600μm diameter particles representative of the sizes that actually occur in erosion environments were used so that the extent of the damage caused by individual impacts would not overwhelm the mechanism that was occurring. It was felt that when several millimeter bee-bees were used to be able to locate individual impacts, forces occurred at the metal surface that were so much greater than those produced by actual eroding particles that the resulting mechanism would probably be different.

Sequences of the early portion of the erosion process showing the development of thin platelets of metal are shown in Reference 5. Figure 4 shows a single region of the steady state eroding surface after two subsequent sequences. The platelets that were present at the first sequence are shown in the upper photo. The lower photo shows the marked changes that occurred after the next sequence of erosion. The platelets in the upper right part of the photo have been knocked off as has the platelet that sat astride the light line extending along the lower right side of both photos. New platelets have been extruded out from the main area of platelets in the center, left side of the lower photo. These observations formed the basis for the development of the platelet mechanism of erosion.

All of the evidence in Reference 5 was developed using aluminum alloys which have a FCC crystallographic structure and many active slip systems. In order to determine whether the formation of platelets is unique to metals of this type, several steel alloys were eroded and their surface microstructures were observed. The alloys tested, 1020, 4340 and 304SS, at various heat treat conditions, formed platelets similar in size, shape and quantity to those initially observed in aluminum alloys.[6] Figure 5 shows the eroded surfaces of 1020 plain carbon steel which has a BCC crystallographic structure with only a few active slip systems after erosion at impingement angles of 30^{o} and 90^{o}. It can be seen that the same mechanism of platelet formation occurs at both angles, thereby accounting for the significant amount of erosion that is measured at $\alpha = 90^{o}$.

The loss of metal from an eroding surface appears to occur by a combined extrusion-forging mechanism. Evidence has been obtained that indicates that the platelets are initially extruded from shallow craters made by the particle impact.[5] Once formed they are forged into a distressed condition as shown in Figure 6 in which condition they are vulnerable to being knocked off the surface in one or several pieces.

Evidence of extrusion being the initiating mechanism of platelet erosion was obtained in an experiment where a thin, 3μm, layer of copper was plated on a 1020 steel substrate which was subsequently eroded with a few SiC particles. Figure 7 shows a cross section of the eroded surface area. Copper can be seen beneath the surface in the center of the photo, indicating that the steel had been extruded over it from the nearby shallow crater. A close examination of the photo shows that there is a thin layer of copper remaining on the surface of the craters. It can be more easily seen in a colored photo.

Figure 8 is a sketch of a proposed sequence of particle impacts that could cause the micrograph of Figure 7. The lip of platelet extruded out of the crater by the first impact is identical to one shown by Gulden and Kubrych.[7] Similar extruded lips are shown in several of the papers of Hutchings.[8] It can be seen that the sequence of extrusion followed by forging of the extruded material can readily account for the surface and sub-surface locations of the copper plating. The presence of the thin layer of copper over the entire surface of the craters in Figure 7 indicates that it is extrusion that

forms the lips of the platelets rather than micro-machining, as machining would have removed the thin copper layer. Other evidence of the extrusion process using a 300 Å thick gold layer on the surface is presented in Reference 5.

Figure 9 is a sequence of photos that shows the extrusion formation of a single platelet, its subsequent spreading by forging and, finally its removal as the result of a particle striking it.[5] The target alloy was 7075-T6 Al. The sequence occurs in clockwise order starting from the upper left photo. The curved striations in photo 1 are covered over by the large platelet that was formed by one particle striking the right side of the metal, shown in photo 2. The platelet was extruded from the straight line, striated, shallow crater and flipped over the top of the crater formed earlier that has curved striations in its surface. The striations on the surfaces of the craters are imprints of striations that form on the fracture surfaces of the SiC particles used to erode the aluminum.

The lower right photo, 3 in Figure 9 shows how two subsequent particle strikes in the area forged the platelet out to a larger size with a sub-platelet forming at its upper left side. In the fourth photo the platelet has been knocked off the surface and the crater surface with the curved striations and a portion of the straight striations of the crater out of which the platelet was formed can be seen. The deep curved striation can be easily seen in photos 1 and 4 to identify that it is the same surface which was covered over by the platelet in photos 2 and 3.

The platelets do not adhere to the surfaces over which they are extruded. Rather they adhere to some location along the extrusion path. In the case of the platelet shown in photo 2 of Figure 9, it is attached at the point where its right side is next to the crater from which it was extruded. In photo 3, the attachment point is now under the forged out platelet, making a mushroom type configuration. The amount of plastic deformation represented by these photos is large and could probably only have occurred on such a low elongation (11%) alloy as 7075-T6 Al if it occurred at an elevated temperature.

Two examples of the shapes of platelets formed on the surface of eroding ductile metals are shown in Figures 10 and 11. Figure 10 shows at low magnification the cross section of the eroding surface of 310SS tested at an elevated temperature. Platelets can be seen along the surface. The lower, higher magnification photo of the platelet between the two polishing marks in the upper photo shows a distressed, mushroom shaped platelet whose stem is cracked. This platelet is very near to being removed, probably by only one or two more particle impacts.

Fig. 11 shows the cross section of a 1020 steel specimen tested in an oxidizing atmosphere at an elevated temperature. The large platelet shown is surrounded by iron oxide formed during the test. The oxide helped to maintain the thin platelet on the surface through the polishing steps used in preparing the specimen for metallographic examination.

The effect of particle velocity on the rate of erosion of ductile alloys is well known.[2] The effect of velocity on the platelet formation process is shown in Figure 12 along with the resultant erosion rates. The 1020 steel was tested at 25°C. The cross section of the eroded surface in the left photo shows several platelets of different configurations that occurred at a particle velocity of 30 m/s. The mushroom shaped platelet on the left side of the photo is typical of the type shown in Figure 6 and is similar to the platelet cross section shown in Figure 10. The cross sections of platelets formed at a velocity of 130 m/s are shown in the right photo for a velocity of 130 m/s. The increased size of the platelets is caused by the marked increase in the force imparted to the surface by the much faster moving particles, which results in the increase in the erosion rate from 0.94 to 12.4 $cm^3/gx10^{-5}$. The increased particle velocity did not change the erosion mechanism, but only the sizes of the platelets.

The beginning portion of the incremental erosion rate curve was investigated using several alloys and testing conditions. A typical set of curves for 1018 steel is shown in Figure 13. It can be seen that there is an early erosion peak that occurs at all three impingement angles tested. The reason for this peak can be seen in Figure 14 which shows the eroded surface at both the early peak and later steady state conditions. In the upper picture larger craters and platelets can be seen on the surface at the peak erosion rate compared to the size of the craters and platelets of the steady state condition material shown in the lower photo. The larger size

platelets result in the peak erosion rates shown in Figure 13.

The reason for the peak in the incremental erosion curve can be explained using the platelet mechanism of erosion and, in turn, helps to substantiate the concept of the mechanism. At the beginning of the erosion process the early particle impacts occur on relatively undeformed material and larger craters and resultant platelets can be formed. These larger platelets protrude relatively high above the metal surface and are vulnerable to being struck by succeeding particles and knocked off the surface. As the erosion process continues the overlapping of craters and platelets occurs, resulting in the forming of smaller craters and platelets. Many of these platelets are deformed down into nearby craters where they are harder to knock off the surface. With their size and protrusion up above the plane of the metal surface reduced, they are less vulnerable to being struck by succeeding particles. The larger, more vulnerable platelets that form early in the erosion process result in a peak of weight loss when they are knocked off. The smaller, less vulnerable platelets that are present at steady state conditions result in a lower erosion rate when they are knocked off the surface.

Surface Heating

While there is no direct evidence of heating of the eroding surface on any of the micrographs shown, considerable evidence was gathered during the course of the investigation that temperatures near the recrystallization temperature occurred at the immediate eroding surface.[4] Considerable recent work and some older work in the literature supports the fact that adiabatic shear heating and possibly

some frictional heating occurs on the surface during the erosion process. Hutchings and Winter discussed the generation of heat on an eroding surface.[8] They attributed it to adiabatic shear heating when extrusion lips were formed out of craters. Christman and Shewmon show evidence of melting of 7075-T6 aluminum when it was eroded with 5mm steel balls which imparted very high forces and resulting deformation to localized erosion areas.[9] Adiabatic shear bands were observed in the area where melting occurred. Shewmon used the heating of the surface during erosion to calculate the effect of small particles, <100μm, causing reduced erosion rates on metals.[10] Gulden and Kubarych saw evidence of melting on 1095 steel.[7] Brown and Edington used the low melting temperature metals gallium (mp=29°C) and indium (mp=156°C) specifically to show that erosion caused the generation of heat on the eroding surface by melting both the gallium and indium in experiments.[11]

The presence and documentation of platelets on eroding surfaces has been reported extensively in the recent literature. Some investigators called the platelets chips, some flakes, some lips and several called them platelets. In all instances, however, their figures showed configurations that are called platelets in this review. For example all five papers presented in the erosion session at the April, 1981 International Conference on Wear of Materials showed platelet formation on the eroded surfaces.[12] Three of the five papers describe surface heating.

In Reference 7 platelet formation is noted on 2024 Al eroded surfaces. In Reference 13 extensive platelet formation is shown. Platelet formation occurred on copper single crystals as observed by Brown and Edington in Reference 14. Rickerby and MacMillan carefully documented the development of platelets at the intersections of indentations caused by spheres striking the target surface.[15] Christman and Shewmon in their work on the erosion of 7075-T6 aluminum alloy reported the generation of platelets and their removal from the surface as the erosion metal loss mechanism.[16]

Platelet Mechanism Description

A consensus has developed that erosion occurs by the generation and loss from the surface of platelet-like pieces of metal. Combining the observations to formulate a mechanism that considers them has been done in Reference 5. A brief description is presented here for continuity of this review.

Figure 15 is a sketch of a cross section of an eroding ductile metal.[5] The erosion heated surface, 5 - 15μm thick, consists of platelets at various stages of generation and large strain deformation. Beneath the platelet zone is a work hardened zone that developed during the early stages of the erosion exposure. This zone lies beneath the heated surface region and strain hardens as a function of the strain hardening coefficient of the target metal. Beneath the cold worked zone is base metal at whatever condition it was worked or heat treated to.

It is proposed that the following sequence occurs in the erosion process: In the beginning platelets are formed, initially without loss of material. Adiabatic shear heating of the immediate surface region begins to occur. Beneath the immediate surface region, a work hardened zone forms as the kinetic energy of the impacting particles is enough to result in considerably greater force being imparted to the metal than that required to generate platelets at the surface.

When the surface has been completely converted to platelets and craters and the work hardened zone has reached its stable hardness and thickness, steady state erosion begins. The reason that the steady state erosion rate is the highest rate in Figures 1, 17, 18 and 20 is that the sub-surface cold worked zone acts as an anvil to increase the efficiency of the impacting particles, or hammers, to extrude-forge platelets in the now fully heated and most deformable surface region. When the anvil is fully in place and the platelets are fully formed and heated, maximum material removal rates will occur. This cross section of material conditions will move down through the metal as erosion metal loss occurs.

To document the occurrence of a heated surface area that could have reached the recrystallization temperature of the target metal and a sub-surface work-hardened zone, cross sections of eroded aluminum and steel alloy specimens were prepared and microhardness tested using a very light, 5gm, load so as not to cause false readings near the surface.[6] Figure 16 shows the microhardness survey of an 1100-0 aluminum specimen. The lower hardness, immediate surface region that was heated can be seen, particularly for the $\alpha = 30^{\circ}$ impingement angle

where erosion rates are the greatest. The hardness increases to a sub-surface work hardened zone followed by a hardness decrease to that of the base metal. In a paper by Salik and Buckley a micrograph of an eroded 6061 Al cross section is shown that labels the three regions discussed above.[17]

THE EFFECT OF MECHANICAL PROPERTIES ON THE EROSION OF DUCTILE METALS

The platelet mechanism of erosion restructures many of the previously accepted relationships between erosion behavior and physical and mechanical properties of ductile metals. Ductility, strain hardening, malleability and thermal properties become more important, requiring that the effects of such older related properties as hardness and strength be reassessed. Several recent investigations have studied these variables. The results of investigations that varied hardness, strength, toughness, ductility and heat treatments to anneal or harden alloys will be reviewed in this section.

In work by this author several steel and aluminum alloys have been tested at various strength, hardness and ductility levels.[4, 6] In Figure 1 it can be seen that a fine pearlite microstructure with a hardness of R_B 99 erodes some 40% faster at steady state erosion conditions than does the same steel in the softer, R_B 79, more ductile, spheroidized condition.[4] Figure 17 shows the incremental erosion rate curves for 1100-0 aluminum and 7075-T6 aluminum. Both alloys formed the same type and size of platelets when eroded with SiC particles, but the erosion rates are markedly different. The 7075-T6 with a tensile strength of 76,000 PSI eroded 50% faster than the much weaker 1100-0 Al that has a tensile strength of 13,000 PSI. However

1100-0 is much more ductile than the 7075 Al, 35% compared to 11% elongation. In the case of these aluminum alloys, higher ductility results in greater erosion resistance. In tests on 304SS to determine the effects of properties on erosion behavior, it was determined that less ductile, as rolled sheet had a higher erosion rate than annealed sheet.[6]

Higher strength and hardness results in significantly greater erosion rates. It is thought that the more ductile alloys deter erosion by distributing the kinetic energy of impacting particles by plastic deformation of a large region under the surface impact point of a particle, thereby reducing the concentration of force at the surface impact point and, therefore, the extrusion and forging of platelets at that point.

The possible effect of the strain hardening coefficient of three metals is indicated in Figure 18. The amount of erodent required for the three materials tested to reach steady state erosion conditions is inversely proportional to their strain hardening coefficients. Table 2 shows this relationship. A higher strain hardening coefficient results in the formation of the sub-surface, cold worked zone anvil sooner and, hence, steady state erosion is reached with a fewer number of particles having impacted the surface.

In spite of the fact that the stainless steel and OFHC copper form a work hardened layer sooner than the 1020 steel, they erode at much lower rates at steady state conditions, see Figure 18. This appears to relate to the elongation of the alloys as shown in Table 2 and not to their strength. It is realized that the strain rates and

actual deformation temperatures at the eroding surface are greatly different from those of the slow strain rate tensile test that is used to determine elongation. However, tensile elongation as an indication of the ductility of a metal has been able to be related to erosion behavior reasonably well.

Another example of the effect of strain hardening of the sub-surface "anvil" is shown in Figure 19 and 20. In this experiment, the impacting particle was varied and the erosion of annealed 1020 steel determined.[18] A weak mineral particle that fragmented on impact, apatite, and a strong particle that did not, Al_2O_3, were used with all other testing conditions being the same. Figure 19 shows the incremental erosion curve using Al_2O_3 particles. The number of particles to reach steady state was of the order of 50g. Figure 20 shows the curve for the weak, apatite particle. Almost 200g of particles were required to reach steady state erosion even though the level of that steady state erosion was only 25% as great as that which occurred when the Al_2O_3 particles were used.

It was postulated that the reason that the 1020 steel eroded with Al_2O_3 particles reached steady state erosion in less than half the erodant weight it took when using the apatite particles is that the weak apatite fragmented into small particles when they impacted the surface. The effective size of the apatite particles after they broke up was too small with too little available kinetic energy to strain harden the sub-surface layer as effectively as the intact, larger Al_2O_3 particles did. It thus took longer to form an "anvil" in the 1020 steel and it was not as an effective one as that formed by the Al_2O_3

particles. This effect of the breaking up of the apatite on the amount of kinetic energy that is available from its largest fragment may also relate to the particle size effect in erosion.[19] The largest fragments of the apatite were less than the 100μm dia size below which erosion rate is reported to decrease with particle size.

Another relationship between strength and hardness and erosion behavior is shown in Table 3 for 4340 low alloy steel.[6] Four heat treat conditions were used to determine the effect of property levels on the erosion resistance. A change in the room temperature strength from 300KSI to 100KSI UTS and hardness from Rc 60 to Rc 19 had essentially no effect on the erosion resistance. If anything, the lowest strength and hardness condition, the spheroidized condition, had the best erosion resistance. The room temperature elongation variation also did not have much effect on the erosion rate nor did differences in fracture toughness and Charpy impact strength. It is thought that the inability of different quenched and tempered conditions to affect the erosion behavior of the 4340 relates to the heating of the eroding surface. The thermal treatment strengthening of the alloy was negated by the heat generated by the erosion process. Thus, all four test surfaces were near the same heat treated condition while they were eroding.

Table 4 shows the effect of testing above and below the ductile-brittle transition (DBTT) of 1020 steel (-18°C) on its erosion resistance.[16] The low temperature test was run by strapping the specimen to a piece of dry ice (mp -78°C) before inserting it in the erosion tester. It can be seen that the erosion rate goes up

considerably when the steel is tested below its DBTT where it only has 1 - 5% elongation, compared to 25% elongation in its above DBTT, more ductile condition.

There is considerable evidence in the recent literature to support the idea that higher strength and hardness do not generally result in greater erosion resistance within families of alloys. Gulden, found that there was no difference in the erosion rates of 1095 steel specimens tested over a tensile strength range of 3 times.[20] These results compare favorably with those determined in the 4340 tests reported in Table 3. Both test series were tested at a 30° impingement angle. However, at a 90° impingement angle she found that the lowest strength and hardness heat treat conditions (Rc 30) resulted in a considerably lower erosion rate compared to the highest hardness (Rc 66) condition. This further indicates the beneficial effect of greater ductility on erosion resistance.

In Reference 7 Gulden reported that 2024-T6 aluminum eroded considerably more than the weaker but more ductile 2024-T6 aluminum. This compares with the results shown in Figure 17 comparing 7075-T6 with 1100-0 aluminum. In tests on 1095 steel she measured erosion rates that were 2-1/2 times higher for the Rc 66 full hard condition compared to the Rc 20 annealed condition.[7] However, in erosion tests of binary Fe-Cr alloys that were hardened by solid solution strengthening rather than the strained lattice hardening that occurs in the 1095 steel, she observed that erosion resistance did vary directly with hardness.

In Reference 17 it was reported that there was no correlation between the hardness varied by heat treatment and the erosion behavior of 6061 aluminum and 1045 steel. In these alloys, the lattice is strained by precipitation hardening (6061 Al) and martensite formation (1045 steel) to achieve the higher hardness with an attendant decrease in ductility. In References 10 and 16 Shewmon reported that higher hardness or fracture toughness did not enhance erosion resistance. The same effect was reported by the author in Reference 6. Lattice strain hardening effects such as precipitation hardening and martensite formation can be removed by the surface heating that occurs in the erosion process. Solid solution strengthening effects, on the other hand, would not be so effected, as was demonstrated in Reference 7.

Thus a body of evidence is growing that relates higher erosion resistance to the increased ductility of the metal rather than to higher strength and hardness. This behavior correlates well with the platelet mechanism of erosion of ductile metals. The ability to plastically deform to absorb the force from the kinetic energy of the impacting particles so that the local fracture stress of the metal platelets that are formed is not exceeded results in lower erosion rates. However, there is a limit to the effect ductility has on increasing the erosion resistance of a ductile metal at the expense of strength. A point is reached where the strength of an alloy has been reduced to such a low level, albeit with high ductility, that localized fracture stresses can be exceeded at particle impact sites no matter how much of the force is disipated and erosion rates begin to increase with further strength reductions even though the ductility

is still increasing.[6]

CONCLUSIONS

1. The mechanism of erosion of ductile metal alloys by small impacting solid particles occurs by the extrusion and forging of thin platelets which are subsequently knocked off the surface.

2. The ductility of metal alloys as measured by their tensile elongation correlates most closely of all mechanical properties investigated to date with erosion resistance.

3. Strength and hardness of ductile metals, except for solid solution strengthened alloys, do not directly relate to the erosion resistance of the alloys.

4. A sub-surface, cold worked zone which acts as an anvil to increase the erosion efficiency of the impacting particles is developed by plastic deformation resulting from the force applied by the impacting particles.

5. The strain hardening coefficient of alloys relates to how soon the alloy reaches a steady state erosion condition, i.e., the development of its sub-surface cold worked zone, but not to the magnitude of the steady state erosion rate.

ACKNOWLEDGEMENT

This work is supported by the Technical Coordination Staff of the Office of Fossil Energy of the U.S. Department of Energy under Contract Number DE-AC03-76SF00098 through the Fossil Energy Materials Program, Oak Ridge National Laboratory, Oak Ridge, Tennessee.

REFERENCES

1. Finnie, I.; "The Mechanism of Erosion of Ductile Metals"; Proceedings Third U.S. National Congress of Applied Mechanics, ASME: New York, pp. 527-532; 1958.

2. Finnie, I. and McFadden D.; "On the Velocity Dependence of the Erosion of Ductile Metals by Solid Particles at Low Angles of Incidence"; Wear 48 No. 1, pp. 181-190; May 1978.

3. Finnie, I., Wolak, J., Kabil, Y.; "Erosion of Metals by Solid Particles"; Journal of Materials, 2, pp. 682-700; ASME: 1967.

4. Levy, A.V., "The Solid Particle Erosion Behavior of Steel as a Function of Microstructure"; Wear 68 No. 3, pp. 269-288, May 1981.

5. Bellman, R. Jr., and Levy, A.V.; "Erosion Mechanism of Ductile Metals"; Wear 70 No. 1, pp. 1-28; July 1981.

6. Foley, T. and Levy, A.; "The Erosion of Heat Treated Steels", Wear 91 No. 1 pp. 45-64, October 1983.

7. Gulden, M.E. and Kubarych, K.G.; "Erosion Mechanisms of Metals"; Report SR81-R-4526-02, Solar Turbines, Inc. San Diego, California; November 30, 1982.

8. Winter, R. and Hutchings, I.; "The Role of Adiabatic Shear in Solid Particle Erosion"; Wear 34, pp.141-148; 1975.

9. Christman, T. and Shewmon, P.; "Adiabatic Shear Localization and Erosion of Strong Aluminum Alloys"; Wear 54 No. 1, pp. 141-146; May 1979.

10. Shewmon, P.; "Particle Size Threshold in the Erosion of Metals"; Wear 68 No. 2, pp. 253-258; May 1981.

11. Brown, R. and Edington, J.; "The Melting of Metal Targets During Erosion by Hard Particles"; Wear 71 No. 1, pp. 113-118; September 1981.

12. Proceedings of the International Conference on Wear of Materials; ASME; San Francisco, California; March 30-April 1, 1981, pp. 548-596.

13. Brown, R., Jun, E., and Edington, J.; "Mechanisms of Solid Particle Erosive Wear for 90° Impact on Copper and Iron"; Wear 74 No. 1, pp. 143-156; December 1982.

14. Brown, R. and Edington, J.; "Erosion of Copper Single Crystals Under Conditions of 90° Impact"; Wear 69 No. 3, pp. 369-382; July 1981.

15. Rickerby, D. and MacMillan, N.; "The Erosion of Aluminum by Solid Particle Impingement of Normal Incidence"; Wear 60 No. 2, pp. 369-382; May 1980.

16. Christman, T. and Shewmon, P; "Erosion of A Strong Aluminum Alloy"; Wear 52 No. 1, pp. 57-70; January 1979.

17. Salik, J. and Buckley, D.; "Effect of Mechanical Surface and Heat Treatments on Erosion Resistance"; Proceedings of the International Conference on Wear of Materials; ASME: San Francisco, California; March 30 - April 1, 1981.

18. Levy, A.V. and Chik, P.; "The Effects of Erodent Composition and Shape on the Erosion of Steel"; Wear 89 No. 2, pp. 151-162, August 1983.

19. Tilly, G.P.; "A two Stage Mechanism of Ductile Erosion"; Wear 23, pp. 87 - 96, 1973.

20. Gulden, M.E.; "Influence of Brittle to Ductile Transition on Solid Particle Erosion Behavior"; Proceedings of the Fifth International Conference on Erosion by Liquid and Solid Impact; Cambridge, England; September 1979.

TABLE 1

EFFECT OF COLD WORK ON THE INITIAL EROSION RATE

OF SPHEROIDIZED 1075 STEEL

% Cold rolled	Hardness, VHN 1000 gm. load	Initial erosion rate from 60gm. of SiC particles in g/g
0	152	0.98×10^{-4}
20	242	1.03
40	262	1.49
60	288	1.66
80	316	1.72
		steady state erosion rate 2.2

TABLE 2

STRAIN HARDENING EFFECT ON STEADY STATE EROSION

Metal	UTS* in KSI	ELONG.* in 2"	HARDNESS* RB	STRAIN° HARDENING COEFF.	APPROX. WEIGHT OF PARTICLES TO REACH STEADY STATE EROSION IN GRAMS
1020 Steel	65	36	79	0.1	200
OFHC Copper	32	55	--	0.3	100
304SS	84	55	80	0.5	60

* ASM Metal Process Data Book 1981

° R. Hertzberg; "Deformation of Engineering Materials", Wiley, New York, 1976

TABLE 3

EFFECT OF DUCTILITY, STRENGTH, TOUGHNESS, HARDNESS

ON EROSION BEHAVIOR OF 4340 STEEL

HEAT TREAT CONDITION	UTS in KSI	HARDNESS Rc	K_{1c} in KSI in	ELONG. in %	CHARPY IMPACT STRENGTH in ft lbs	STEADY* STATE EROSION in mg
as-quenched	307	60	34	8	10	1.03
200°C	273	53	58	11	16	0.97
500°C	182	39	62	14	12	0.97
spheroidize anneal	∿100	∿19		∿25		0.90

*Statistical average of weight loss per 30gm load of 140μm Al_2O_3 particles at steady state erosion.

$\alpha = 30$ V = 30 mps

T = 25°C

TABLE 4

EFFECT OF DBTT OF 1020 CARBON STEEL ON EROSION

TEST TEMPERATURE	ELONG. in %	STEADY STATE EROSION* in mg
25°C	25	0.25
∿ -78°C (DBTT= -18°C)	1-5	0.82

Statistical average of incremental weight loss per 30gm load of 140μm Al_2O_3 at steady state

$\alpha = 90°$ V = 30 mps

T = 25°C

FIGURES

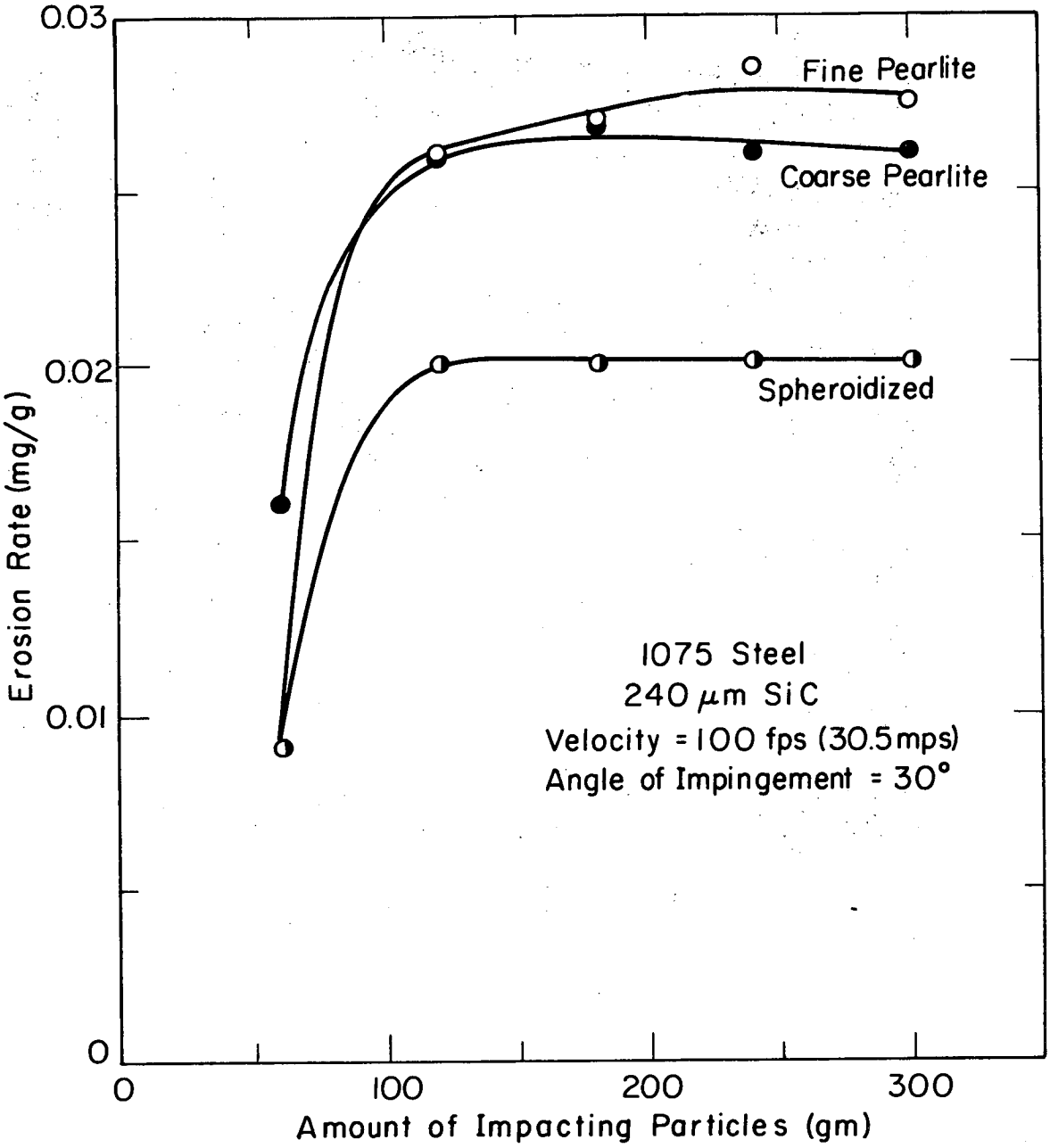

Fig. 1. Incremental erosion of 1075 steel to steady state rate.

XBL775-5486

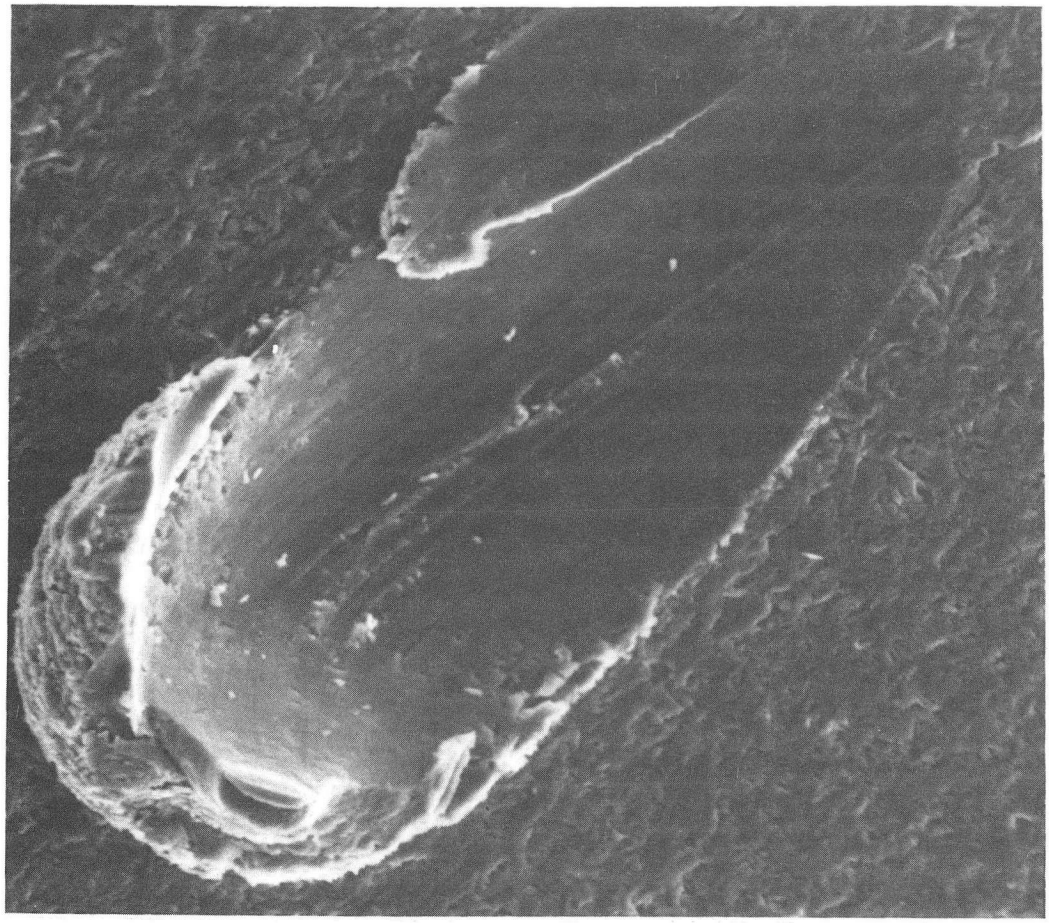

Fig. 2. Single particle impact crater on 1100-0 Al. 1000X

XBB 750-8747

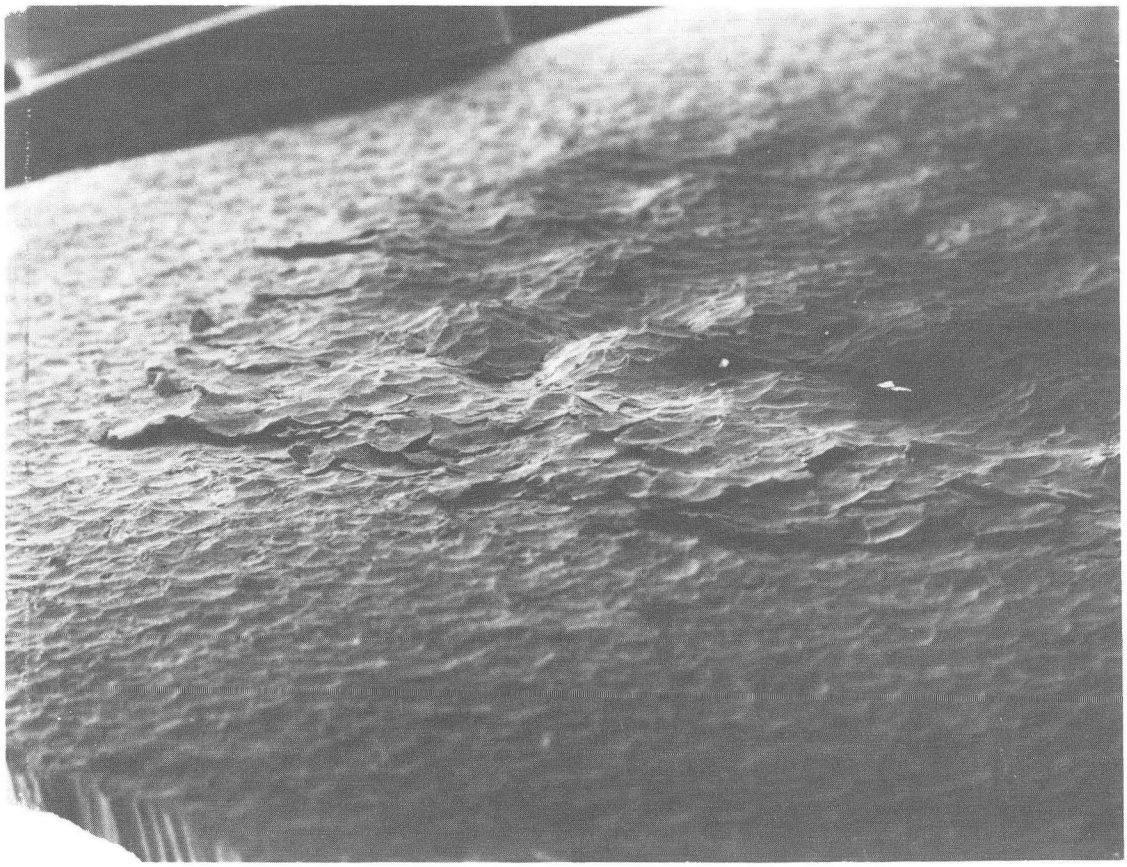

Fig. 3. Platelets at edge of primary erosion zone of 1100-0 Al. 20X

XBB 780-13772

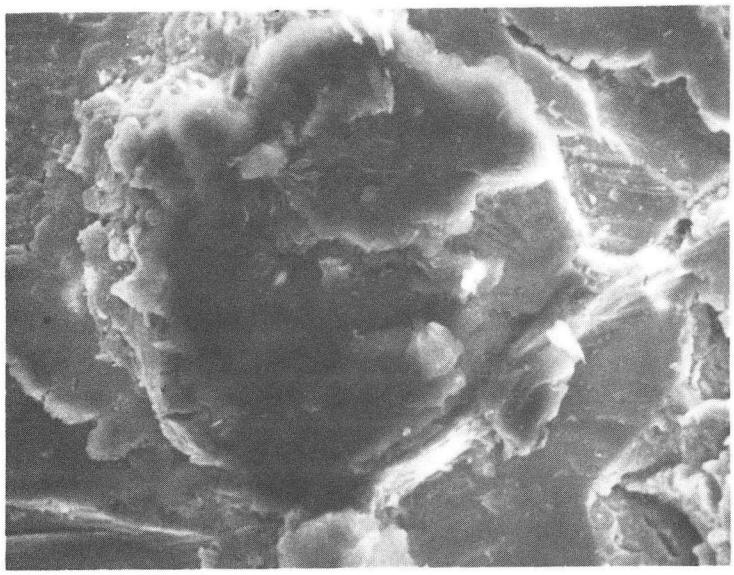

A

10 μm

1g

IMPACT DIRECTION

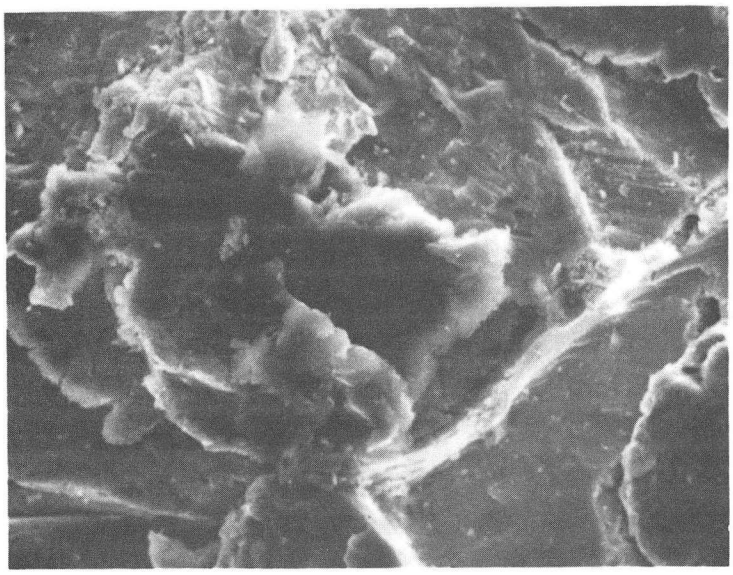

B

10 μm

2g

Fig. 4. Development and loss of platelets on eroded 7075-T6 Al.

XBB 790-13307A

SPHEROIDIZED AISI 1020 STEEL

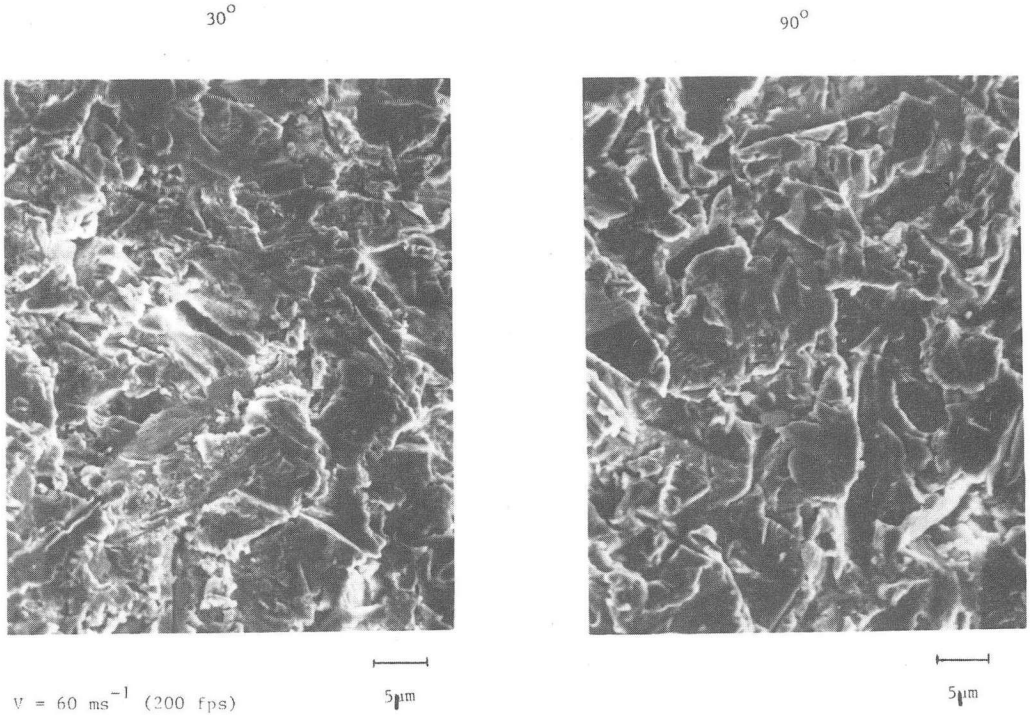

V = 60 ms^{-1} (200 fps)

140 μm Al_2O_3

Fig. 5. Eroded surface of spperoidized 1020 steel at $\alpha=30^{\circ}$ and 90°.

XBB 825-4372

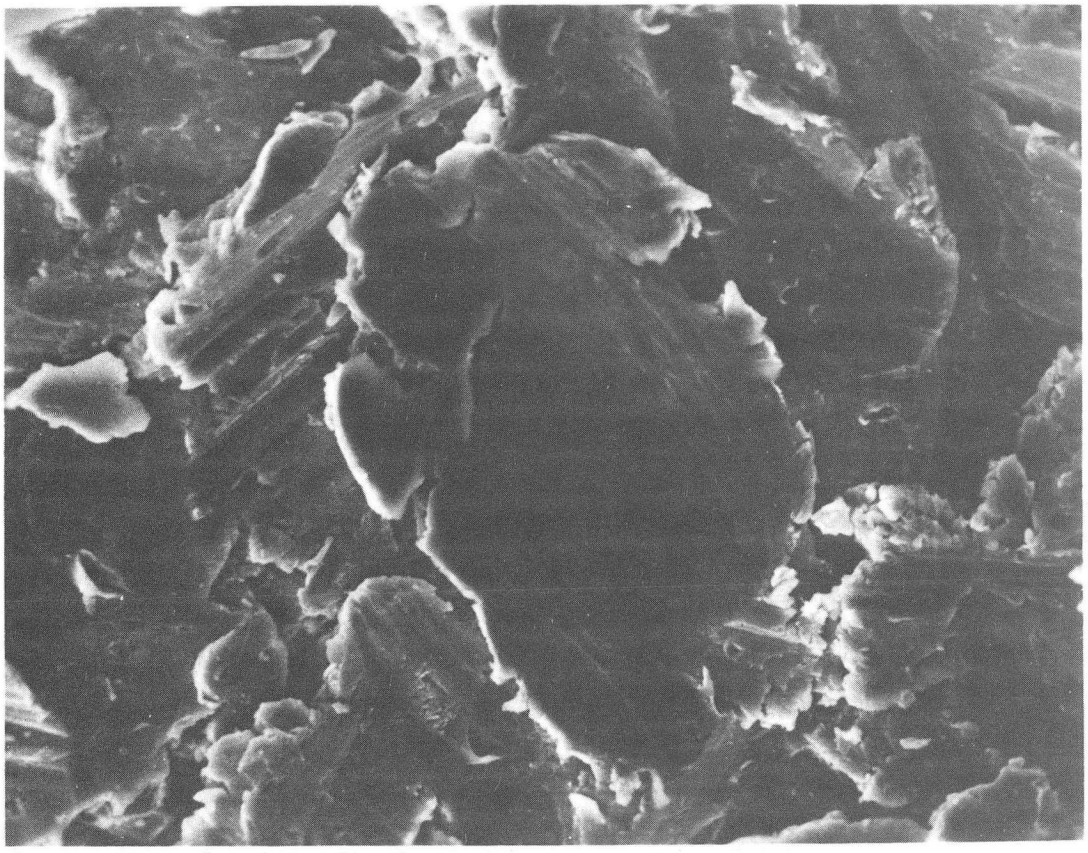

Fig. 6. Erosion platelet on 7075-T6 Al.

10 μm

XBB 806-7866

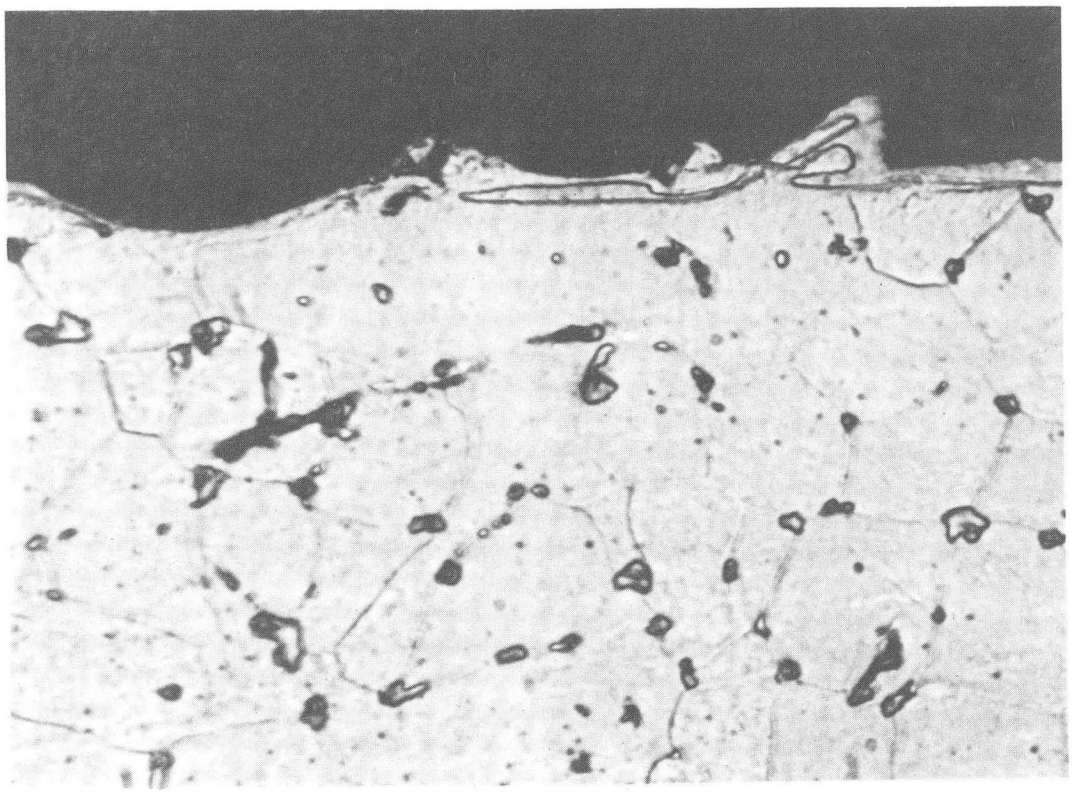

Fig. 7. Cross section of eroded surface area of copper plated steel.

CBB 790-12833A

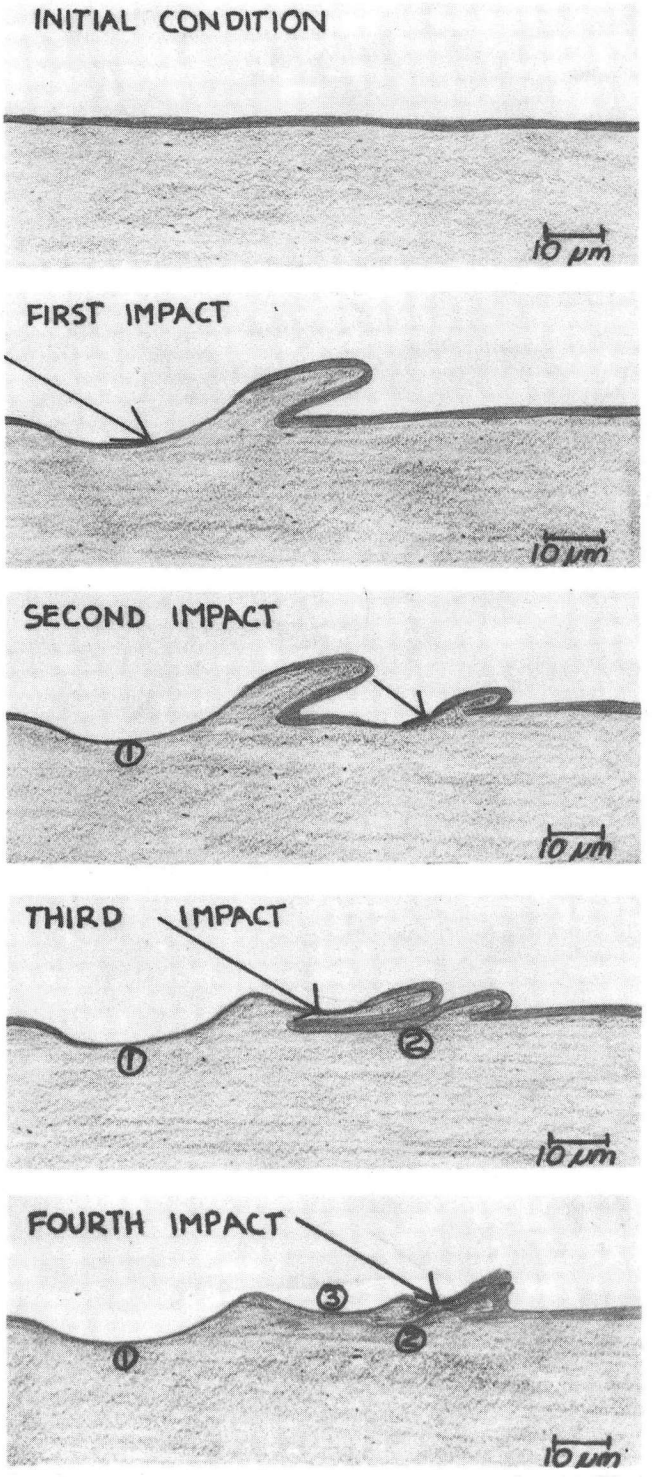

Fig. 8. Proposed sequence of erosion of copper plated steel specimen.

CBB 823-1717

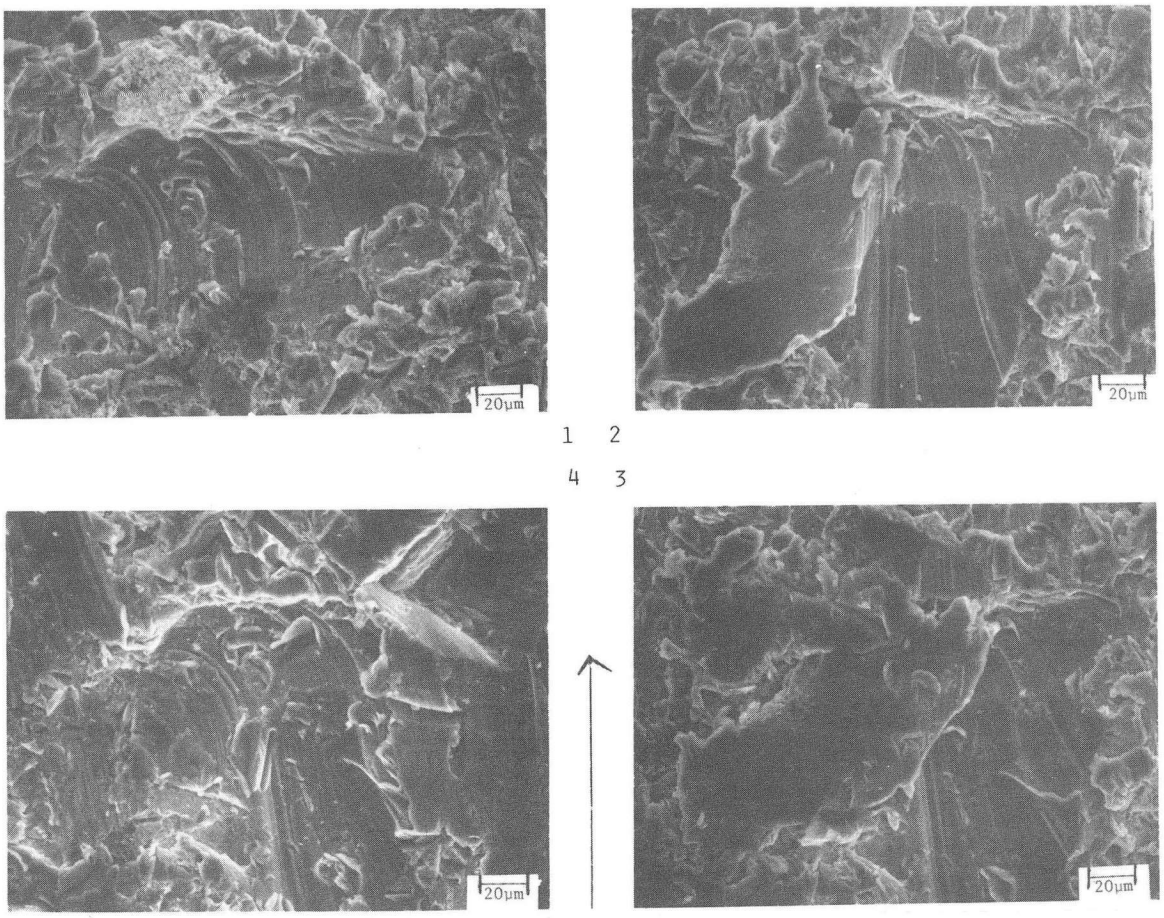

Fig. 9. Sequence of platelet formation and removal on 7075-T6 Al.

XBB 801-1299

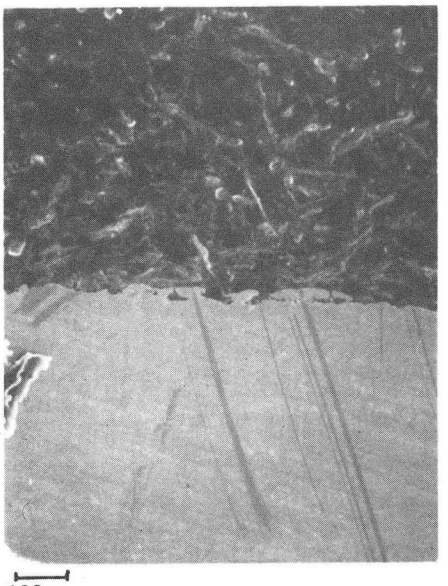

310 STAINLESS STEEL
30° IMPINGEMENT ANGLE
710°C
CROSS SECTIONAL VIEW

Fig. 10. Cross section of 310SS eroded surface showing platelets.

XBB 824-3330

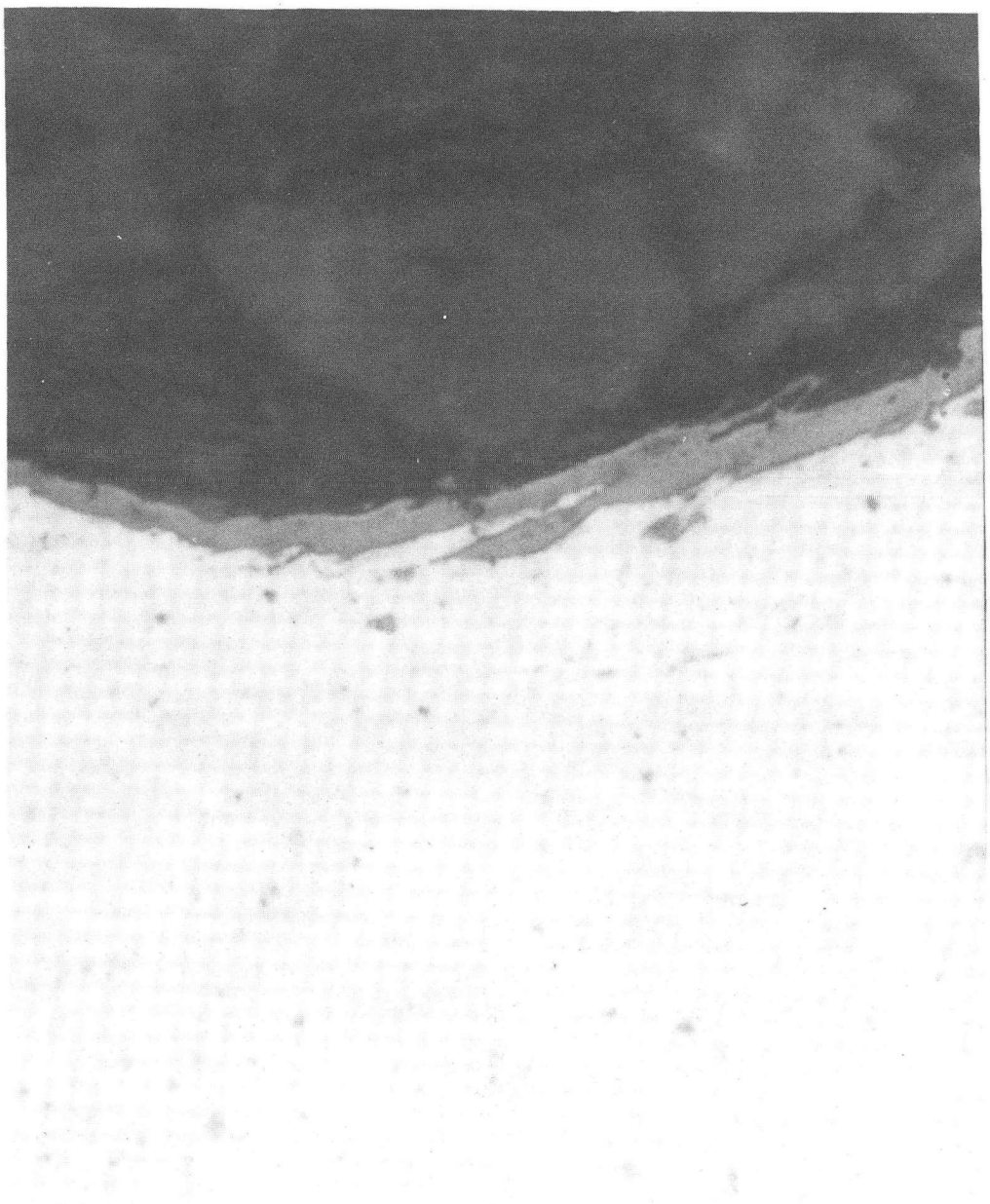

Fig. 11. Cross section of platelets formed on 1020 steel.

10 μm

XBB 821-308

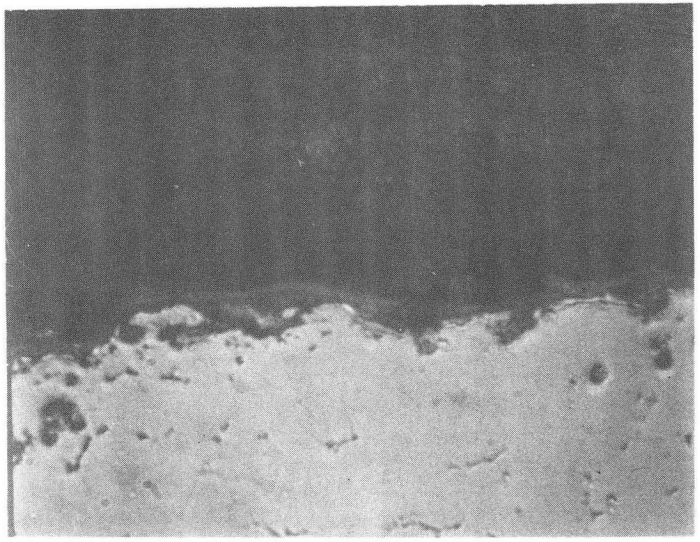

α = 90
v = 30 m/s

10μm

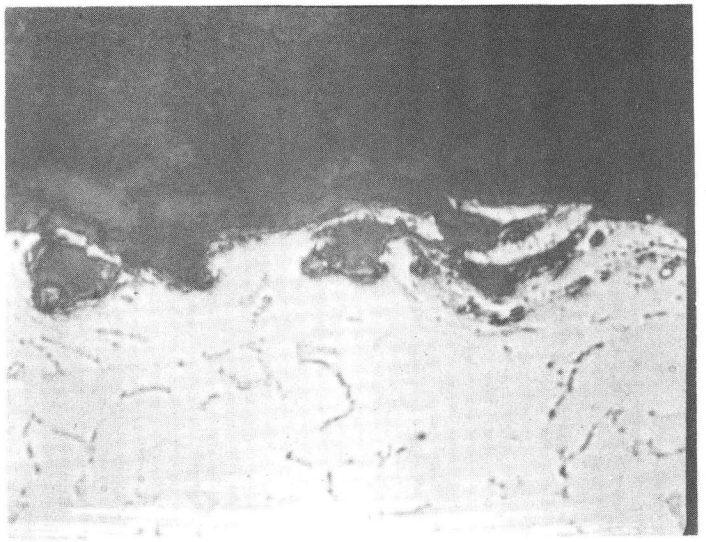

α = 90
v = 130 m/s

10μm

XBB 831-430

Fig. 12. Cross section of 1020 steel eroded by SiC particles at V=30, 130 m/s.

1020 Steel
250 μm SiC

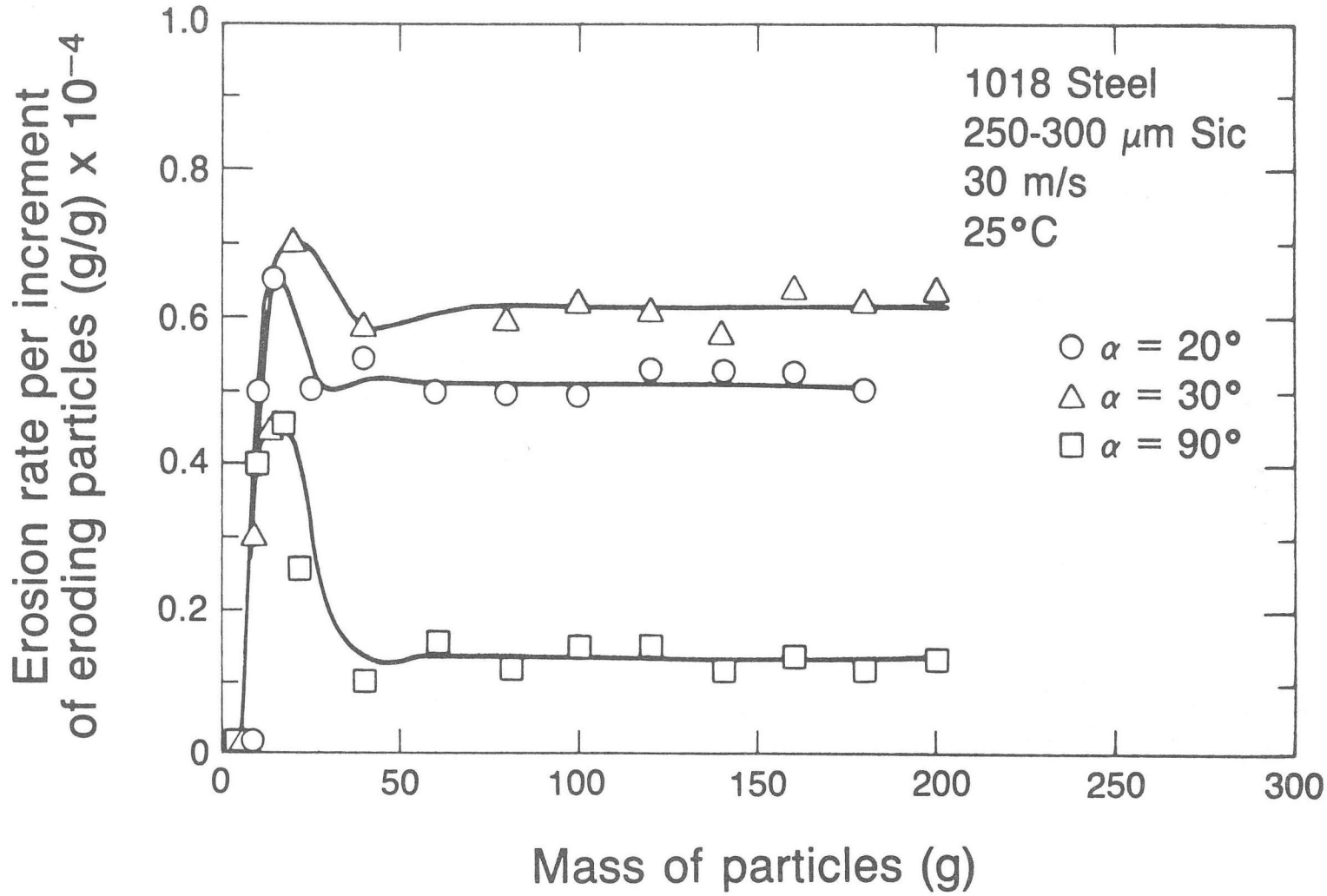

Fig. 13. Incremental erosion rate curve for 1018 steel at α=20,30,90°.

XBL 841-6741

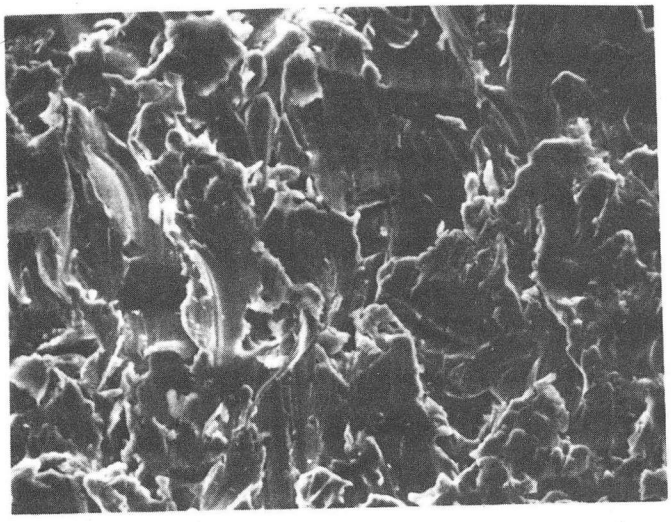

Peak Erosion

10 μm

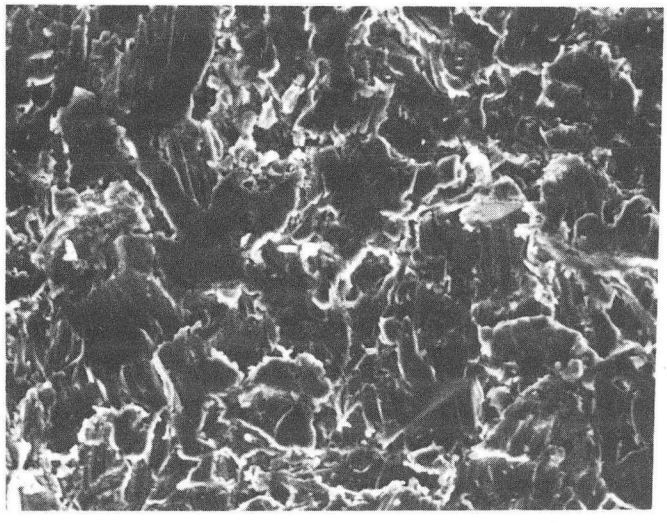

Steady State Erosion

10 μm

Fig. 14. Surface of eroded 1018 steel at peak and steady state erosion conditions.

1018 Steel
30 m/s
250-300 μm SiC
$\alpha = 20°$
25°C

XBB 838-7182

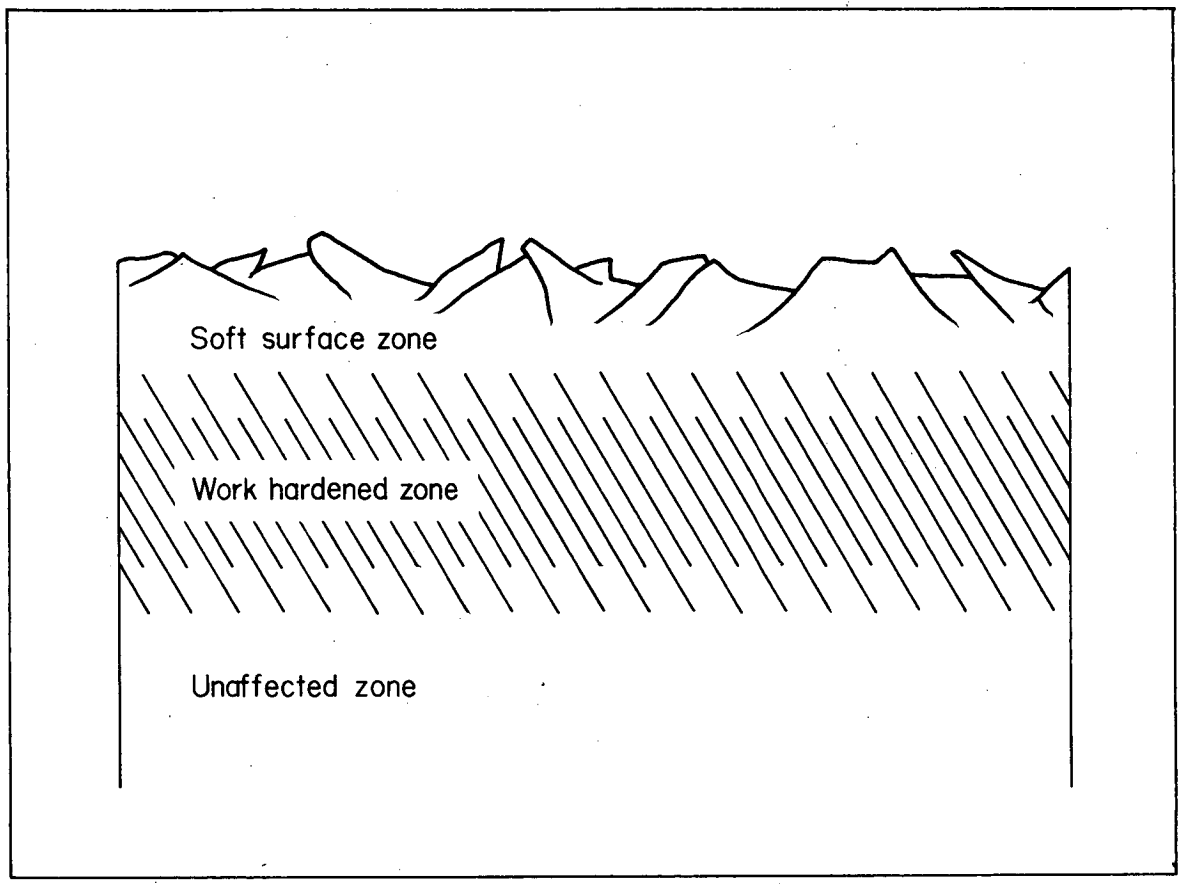

Fig. 15. Sketch of cross section of eroding metal surface.

XBL 807-10669

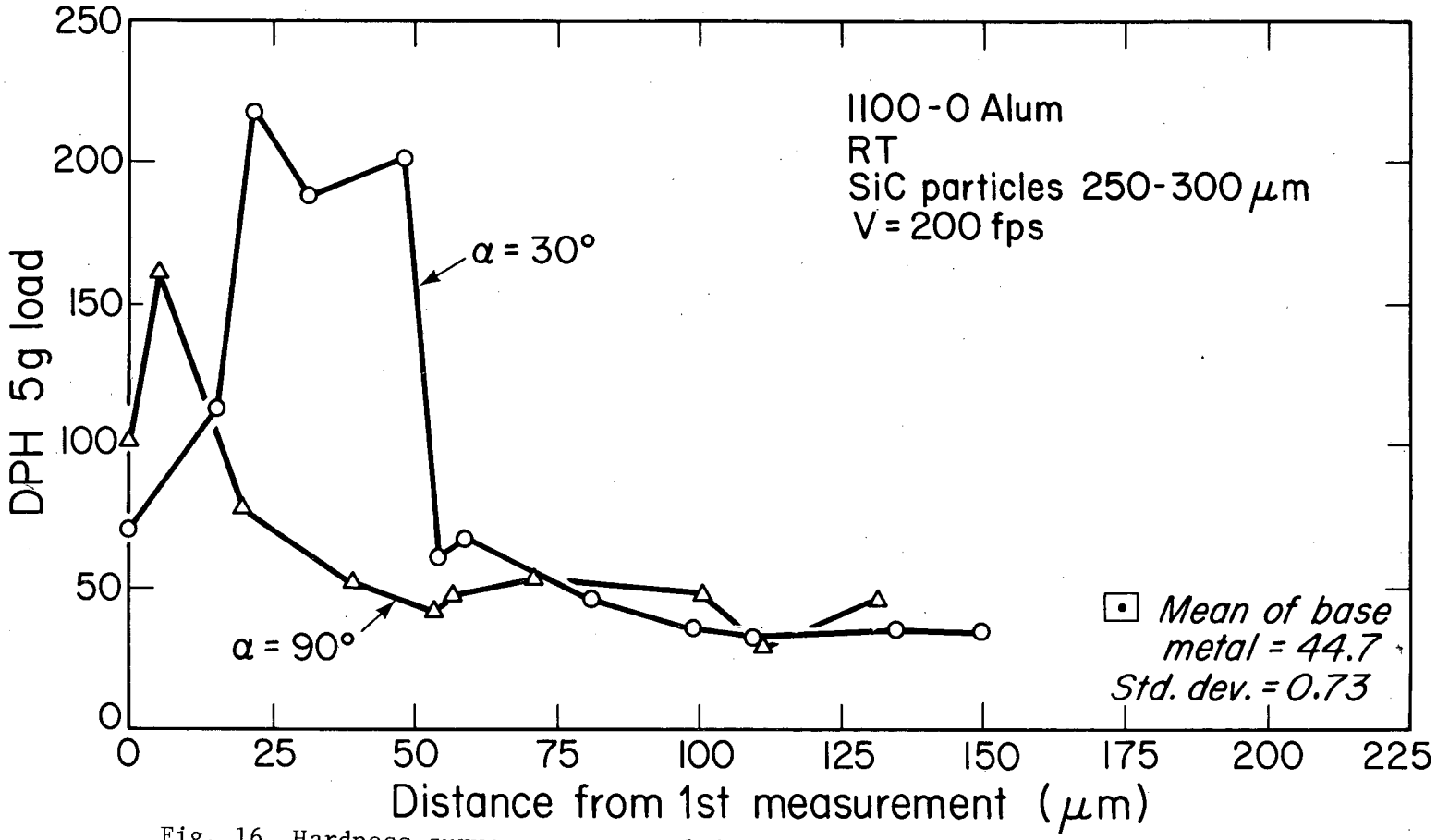

Fig. 16. Hardness survay across eroded material surface region.

XBL 8011-2236

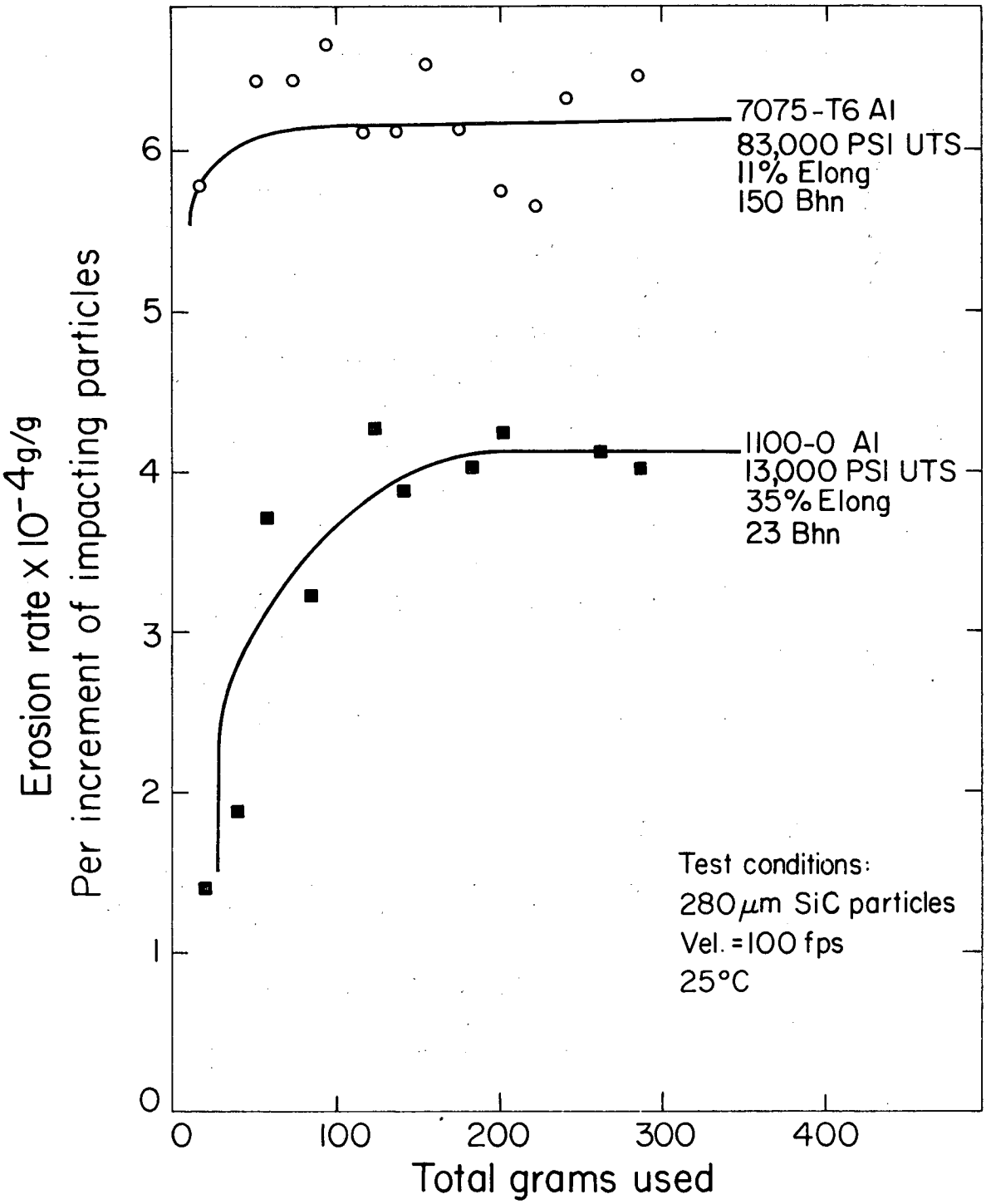

Fig. 17. Erosion rate of 7075-T6 and 1100-0 aluminum.

XBL 8110-1379

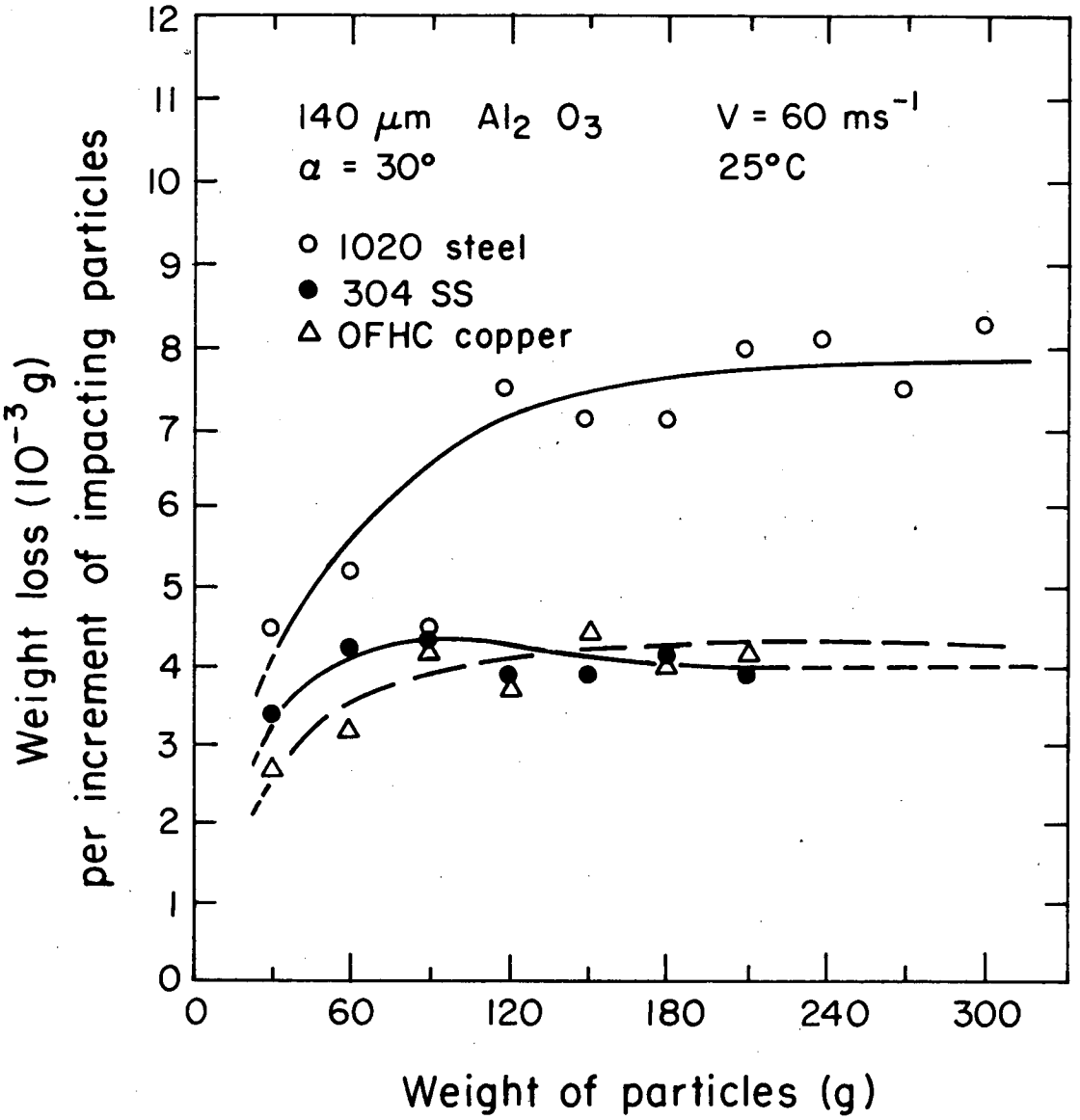

Fig. 18. Incremental erosion rate curves for 1020 steel, 304SS, OFHC copper.

XBL 829 – 1133

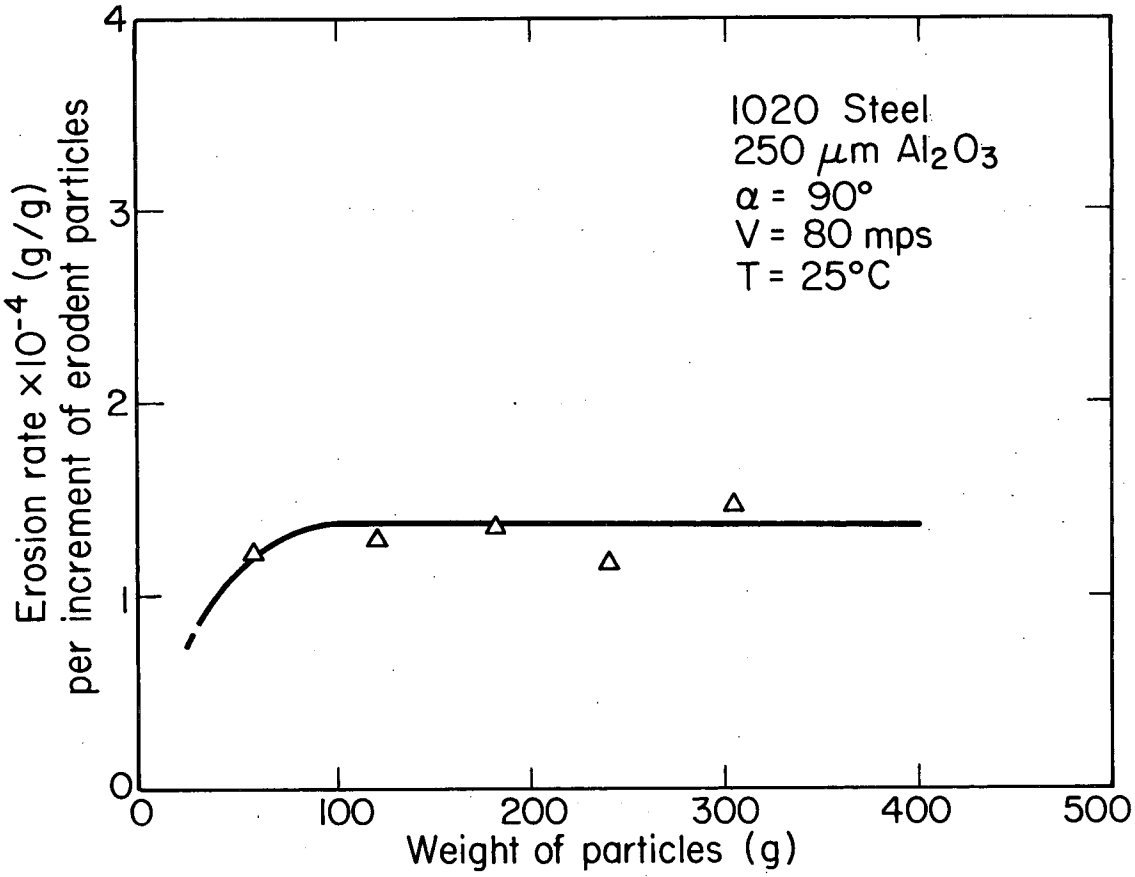

Fig. 19. Erosion rate of 1020 steel using Al_2O_3 particles.

XBL 825-696

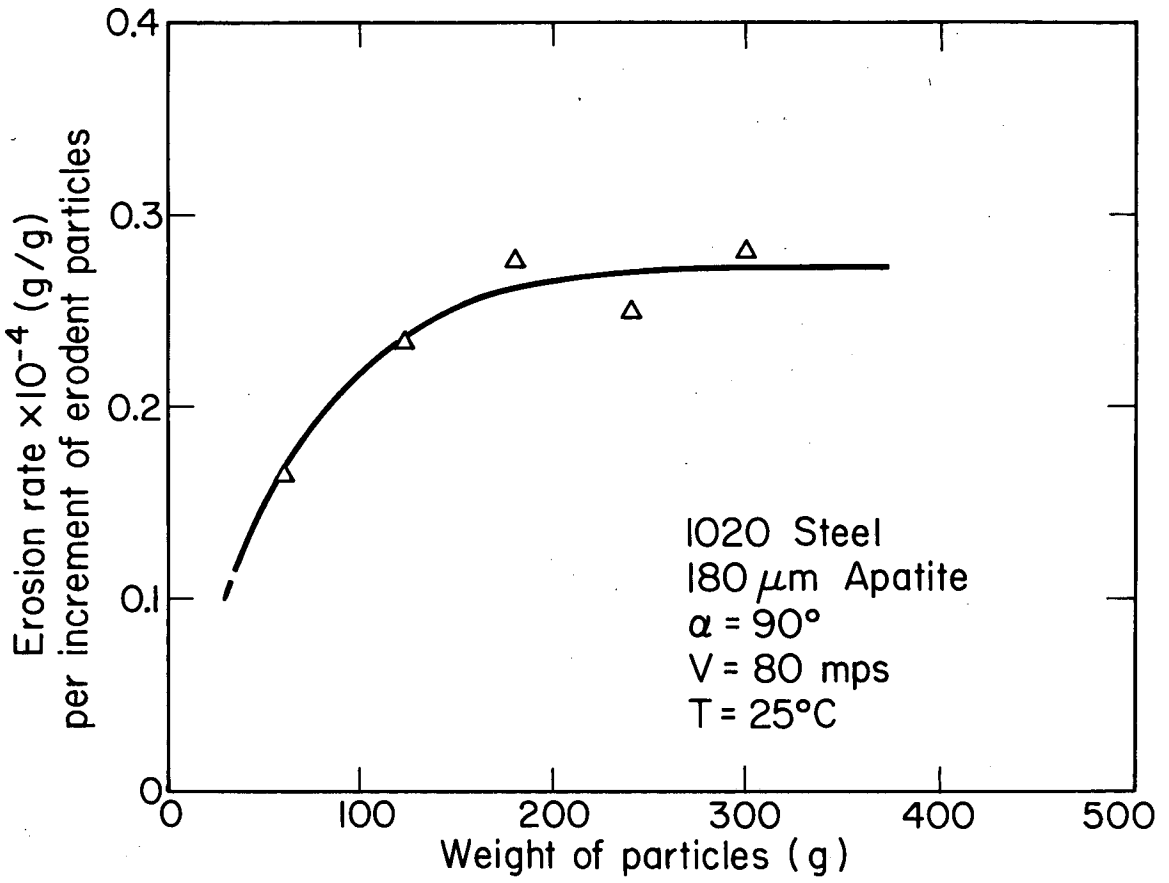

Fig. 20. Erosion rate of 1020 steel using apatite particles.

XBL 825-694

DISTRIBUTION LIST

Wate Bakker
EPRI
3214 Hillview Avenue
P.O. Box 10412
Palo Alto, CA 94304

B.R. Banerjee
Ingersoll-Rand Company
P.O. Box 301
Princeton, NJ 08540

K.L. Baumert
Air Products & Chemicals, Inc.
P.O. Box 538
Allentown, PA 18105

S.M. Benford
NASA Lewis Research Center
21000 Brookpark Road
Cleveland, OH 41135

A.E. Biggs
Arco Chemicals
3801 W. Chester Pike
Newtown Square, PA 19073

R. Blickensderfer
Bureau of Mines
P.O. Box 70
Albany, OR 97321

R.A. Bradley, Manager
Fossil Energy Materials Program
Oak Ridge National Laboratory
P.O. Box X
Oak Ridge, TN 37830

Richard Brown
Materials Laboratory
Department of Chemical Engineering
University of Rhode Island
Kingston, RI 02881

DISTRIBUTION LIST cont'd

D.H. Buckley
NASA Lewis Research Center
21000 Brookpark Road
Cleveland, OH 41135

P.T. Carlson, Task Leader
Fossil Energy Materials Program
Oak Ridge National Laboratory
P.O. Box X
Oak Ridge, TN 37830

J. Carpenter
ECUT Program
Oak Ridge National Laboratory
P.O. Box X
Oak Ridge, TN 37830

J.P. Carr
Department of Energy, Office of Fossil Energy
FE-42 Mailstop 3222-GTN
Washington, DC 40525

Hans Conrad
Materials Engineering Department
North Carolina State University
Raleigh, NC 27659

P. Crook
Cabot Corporation
Technology Department
1020 W. Park Avenue
Kokomo, IN 46901

S.J. Dapkunas
Department of Energy, Office of Fossil Energy
Technical Coordination Staff FE-14
Mailstop C-156 GTN
Washington, DC 40525

DOE Technical Information Center
P.O. Box 62
Oak Ridge, TN 37830

W.A. Ellingson
Argonne National Laboratory
9700 South Cass Avenue
Argonne, IL 60439

DISTRIBUTION LIST cont'd

J. Gonzales
GTE
Chemical & Metallurgical Division
Hawes Street
Towanda, PA 18848

Å. Hammarsten
Teknikum
P.O. Box 534, S-751 21
Uppsala
SWEDEN

E. Haycock
Westhollow Research Center
Shell Development Company
P.O. Box 1380
Houston, TX 77001

J.M. Hobday
Department of Energy
Morgantown Energy Technology Center
P.O. Box 880
Morgantown, WV 26505

E.E. Hoffman, Manager
National Materials Program
Department of Energy
Oak Ridge Operations
P.O. Box E
Oak Ridge, TN 37830

J.A.C. Humphrey
Mechanical Engineering Department
University of California
Berkeley, CA 94720

I.M. Hutchings
University of Cambridge
Department of Metallurgy
Pembroke Street
Cambridge
ENGLAND

Sven Jansson
Stal-Laval Turbin AB
Finspong S-61220
SWEDEN

DISTRIBUTION LIST cont'd

R.R. Judkins
Fossil Energy Materials Program
Oak Ridge National Laboratory
P.O. Box X
Oak Ridge, TN 37830

M.F. Keshavan
Union Carbide Corporation
Coating Services Department
1500 Polco Street
Indianapolis, IN 46224

T. Kosel
University of Notre Dame
Dept. of Metallurgical Engineering
& Materials Science
Box E
Notre Dame, IN 46556

L. Lanier
FMC-Central Engineering Laboratory
1185 Coleman Avenue
Santa Clara, CA 95052

N.H. MacMillan
Pennsylvania State University
167 Materials Research Laboratory
University Park, PA 16802

P.K. Mehrotra
Kennemetal Inc.
1011 Old Salem Road
Greensburg, PA 15601

Ken Magee
Bingham-Williamette Co.
2800 N.W. Front Avenue
Portland, OR 97219

T. Mitchell
Case Western Reserve University
Department of Metallurgy
Cleveland, OH 44106

Fred Pettit
Dept. of Metallurgy & Materials Engineering
University of Pittsburgh
Pittsburgh, PA 15261

DISTRIBUTION LIST cont'd

R.A. Rapp
Metallurgical Engineering
116 W. 19th Avenue
The Ohio State University
Columbus, OH 43210

D.A. Rigney
Metallurgical Engineering
116 W. 19th Avenue
The Ohio State University
Columbus,OH 43210

A.W. Ruff
Metallurgy Division
National Bureau of Standards
B-266 Materials
Washington, DC 20234

Alberto Sagüés
IMMR - University of Kentucky
763 Anderson Hall
Lexington, KY 40506

Gordon Sargent
University of Notre Dame
Dept. of Metallurgical Engineering & Materials Science
Box E
Notre Dame, IN 46556

Paul Shewmon
Dept. of Metallurgical Engineering
116 W. 19th Avenue
Columbus, OH 43210

Gerry Sorell
EXXON Research & Engineering Company
P.O. Box 101
Florham Park, NJ 07932

John Stringer
University of California
Lawrence Berkeley Laboratory
Mailstop 62/203
Berkeley, CA 94720

Widen Tabakoff
Dept. of Aerospace Engineering
University of Cincinnati
Cincinnati, OH 45221

DISTRIBUTION LIST cont'd

Edward Vesely
IITRI
10 West 35th Street
Chicato, IL 60616

J.J. Wert
Metallurgy Department
Vanderbilt University
P.O. Box 1621, Sta. B
Nashville, TN 37235

J.C. Williams
Dept. of Metallurgy & Materials Science
Carnegie-Mellon University
Schenley Park
Pittsburgh, PA 15213

S. Wolf
Department of Energy
Basic Energy Sciences Office
Division of Materials Sciences
Washington, DC 20545

Ian Wright
Materials Science Division
Battelle Memorial Institute
505 King Avenue
Columbus, OH 43201

C.S. Yust
Metals and Ceramics Division
Oak Ridge National Laboratory
P.O. Box X
Oak Ridge, TN 37830

TECHNICAL INFORMATION DEPARTMENT
LAWRENCE BERKELEY LABORATORY
UNIVERSITY OF CALIFORNIA
BERKELEY, CALIFORNIA 94720